OPEN ACCESS
JOURNAL OF ADVANCED DIELECTRICS
Vol. 13, No. 1 (2023) 2242003 (7 pages)

DOI: 10.1142/S2010135X22420036

Optimization of energy storage properties in $(1-x)Na_{0.5}Bi_{0.5}TiO_3$–$xSr_{0.7}La_{0.2}TiO_3$-relaxed ferroelectric ceramics

Ziyue Ma[*,‖], Jianye Zhu[*,‖], Jianhua Wu[*], Yanhua Hu[†], Xiaojie Lou[‡], Ningning Sun[*], Ye Zhao[*], Yong Li[*,§] and Xihong Hao[*,¶]

[*]*Inner Mongolia Key Laboratory of Ferroelectric-Related New Energy Materials and Devices School of Materials and Metallurgy, Inner Mongolia University of Science and Technology Baotou, Inner Mongolia 014010, P. R. China*

[†]*Department of Chemical Engineering, Ordos Institute of Technology, Ordos Inner Mongolia 017000, P. R. China*

[‡]*Frontier Institute of Science and Technology and State Key Laboratory for Mechanical Behavior of Materials Xi'an Jiaotong University, Xi'an Shaanxi 710049, P. R. China*

[§]liyong3062545@126.com

[¶]xihonghao2022@163.com

Received 13 September 2022; Revised 22 September 2022; Accepted 28 September 2022; Published 27 October 2022

Ferroelectric materials are considered to be the most competitive energy storage materials for applications in pulsed power electronics due to excellent charge–discharge properties. However, the low energy storage density is the primary problem limiting their practical application. In this study, $(1-x)Na_{0.5}Bi_{0.5}TiO_3$–$xSr_{0.7}La_{0.2}TiO_3$ [$(1-x)$NBT–xSLT] ferroelectric ceramics are found to exhibit excellent energy storage performances through a synergistic strategy. As the SLT concentration increases, the relaxation characteristic increases significantly and the breakdown strength increases dramatically from 150 kV/cm to 220 kV/cm. The recoverable energy storage density of the 0.55NBT–0.45SLT ceramic is 2.86 J/cm^3 with an energy storage efficiency of 88% under an electric field of 220 kV/cm. Furthermore, the ceramic with x = 0.45 mol exhibited excellent energy storage stability in the ranges of 20–180°C (temperature) and 1–125 Hz (frequency). These excellent properties demonstrate the potential of $(1-x)$ NBT–xSLT ceramics when used as dielectric capacitors in pulsed power systems.

Keywords: Energy storage; ferroelectric; lead-free ceramics; dielectric; microstructure.

1. Introduction

With the growing requirement for energy storage devices for pulsed power systems, ceramic-based dielectric materials are becoming a focus of interest due to their high power density and excellent stability.[1–11] Basically, total energy storage (W_{tot}), recoverable energy storage (W_{rec}) and energy storage efficiency (η) of dielectric ceramic material can be assessed by the following equations[11–13]:

$$W_{tot} = \int_0^{P_{max}} E dp, \tag{1}$$

$$W_{rec} = \int_{P_r}^{P_{max}} E dp, \tag{2}$$

$$\eta = \frac{W_{rec}}{W_{tot}} \times 100\%, \tag{3}$$

where E, P_{max} and P_r are the applied electric field, maximum polarization and remnant polarization, respectively. Therefore, to obtain excellent energy storage performance, large P_{max}, low P_r and high breakdown strength (BDS) need to be satisfied.[15–17]

Currently, four types of dielectric ceramics are widely used for energy storage applications, namely linear dielectrics (LDs), ferroelectrics (FEs), relaxed ferroelectrics (RFEs) and antiferroelectrics (AFEs).[18–21] Compared to LDs with low P_{max} and FEs with high P_r,[22,23] AFEs with double hysteresis loops and RFEs with slender polarization–electric field (P–E) hysteresis loops are considered to be promising materials for energy storage.[15,24] However, RFEs are considered to be the most desirable ceramic dielectric capacitor material at present due to their environmental advantages. Due to the generation of random electric field (RFS), which disrupts the long-range ordered structure of the relaxation material, polar nanoregions (PNRs) are formed and thus excellent energy storage properties are achieved.[25]

Among the relaxation ferroelectric ceramics, $Na_{0.5}Bi_{0.5}TiO_3$ (NBT)-based ceramic is considered to be the

‖These authors contributed equally to this work.

most competitive lead-free energy storage material by virtue of its excellent P_{max} (>40 μC/cm^2). However, the small BDS and large P_r of pure NBT-based ceramic materials lead to low W_{rec}.[15] Therefore, researchers have tried to improve the energy storage behavior of NBT-relaxed ferroelectric ceramics through component optimization.[12,14,26] Qiao *et al*. introduced $Sr_{0.7}Sm_{0.2}TiO_3$ (SST) in NBT ceramics for replacing Bi^{3+} and Na^+ to avoid oxygen vacancies and to inhibit grain growth. The energy storage properties of $(1-x)Bi_{0.5}Na_{0.5}TiO_3$–$xSr_{0.7}Sm_{0.2}TiO_3$ [$(1-x)$NBT – xSST] RFE ceramics were increased via reducing the tolerance factor (t) to increase the relaxation ferroelectric phase and decreasing the grain size to exhibit large BDS of 283 kV/cm.[27] Lin *et al*. prepared $(1-x)(Na_{0.5}Bi_{0.5})_{0.7}Sr_{0.3}TiO_3 - xBi(Mg_{2/3}Nb_{1/3})O_3$ [$(1-x)$NBT–xBMN] RFE ceramics. Sr^{2+} ions were introduced into the NBT ceramics to disrupt the long-range ordering of the ferroelectrics and attract PNRs generation, while BMN was introduced to suppress P_r.[23] This achieves a synergistic increase in energy storage density and η. The above studies demonstrate that combining fine grain and high densities is important for enhancing the BDS and relaxation behavior of NBT-based RFEs, thus further improving their performance in practical applications.[18,28,29]

In this study, exceptional energy storage density and efficiency were achieved in $(1-x)Na_{0.5}Bi_{0.5}TiO_3 - xSr_{0.7}La_{0.2}TiO_3$ [$(1-x)$NBT – xSLT] ceramics. SLT has a significant effect on the reduction of the grain size, which leads to enhanced BDS and relaxation behavior. Moreover, $(1-x)$NBT – xSLT ceramics are fabricated by tape-casting method, which improves the microstructure and densification of the ceramics. This preparation method effectively increases the BDS of the ceramics and contributes to the desired energy storage performance.[30,31] Further, the results show that excellent energy storage properties are achieved at high electric fields. The potential of NBT-based ceramics when used as dielectric capacitors in pulsed power systems is confirmed by these excellent properties.

2. Experimental Details

The $(1-x)$NBT – xSLT (x = 0.2, 0.3, 0.4 and 0.5) RFE ceramics were obtained via tape-casting technique and conventional solid-state sintering method. The weighed drugs were placed in ethanol and ball milled for 24 h to obtain the original powder. The virgin powder was dried and calcined at 850°C for 4 h. The calcined powder was subjected to secondary ball milling. Subsequently, ethanol, tributyl phosphate, polyvinyl butyral (PVB) binder and plasticizer (polyethylene glycol, phthalate) were added to the ceramic powder and then the mixture was ball milled for 18 h to obtain the cast slurry. Air bubbles were removed from the cast slurry by a vacuum defoamer (TP-08, Beijing Oriental Sun Technology Co., Ltd., China). The slurry was cast onto the film strip substrate by a cast machine (LY-150, Beijing Orient Suntech Co., Ltd., China). The obtained thick films were stacked together (DY-30, Tianjin Technology Co., Ltd., China) and further densified green samples were obtained by cold isostatic pressing technique (U150, Shanxi Jinkaiyuan Co., Ltd.) under high pressure. The samples were calcined at 500°C to burn out the binder and then sintered in a crucible at 1170°C for 3 h. To avoid the volatilization of Na^+ and Bi^{3+} during high-temperature sintering, the samples were encapsulated in calcined powder of the same composition. Finally, the ceramic samples were polished to 100 μm and sputtered with an electrode area of 3.14 mm^2, followed by electrical properties testing.

The phase structures of $(1-x)$NBT – xSLT ceramics were analyzed by an X-ray diffractometer (Bruker D8 Advanced Diffractometer, Germany). The surface morphology of the ceramics was observed by scanning electron microscopy (FE-SEM; ZEISS Supra 55, Germany). Temperature dependence of the dielectric constant (ε_r) and dielectric loss (tanδ) was detected via a computer-controlled LCR meter (TH2828, Tonghui, China). The P–E hysteresis loops at the frequency of 10 Hz were measured by a ferroelectric test system (Radiant Technologies, Inc., Albuquerque, USA).

3. Results and Discussion

The room-temperature X-ray diffraction (XRD) patterns of the $(1-x)$NBT – xSLT ceramics in Fig. 1(a) demonstrate that all ceramics exhibit a pure perovskite structure, and no second phase was observed. The enlarged view of the (200) diffraction peak is shown in Fig. 1(b). No splitting of the (200) diffraction peak was observed for all ceramics, which indicates that the ceramics have a typical pseudo-cubic structure. Additionally, the (200) peak shifts to the lower angle as the SLT content increases, which indicates the expansion of the lattice constant.[18,31]

Figure 2 shows the SEM images and grain size distribution of $(1-x)$NBT – xSLT ceramics. It can be observed that all ceramics have a dense structure and no obvious defects are produced. In addition, the average grain sizes of the different components of the ceramics are 2.54, 2.43 and 2.29 μm,

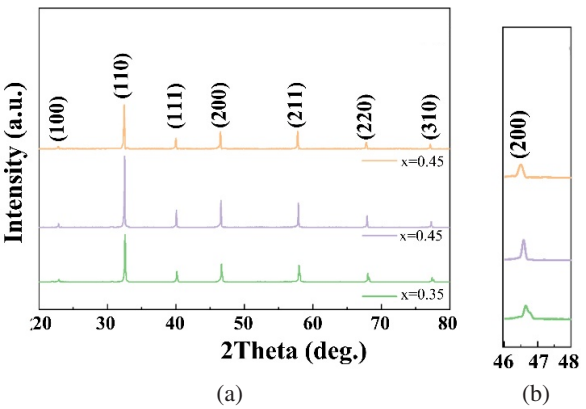

Fig. 1. (a) X-ray diffraction patterns of $(1-x)$NBT – xSLT ceramics in the range of 20–80°. (b) The magnified spectra at (200) peak.

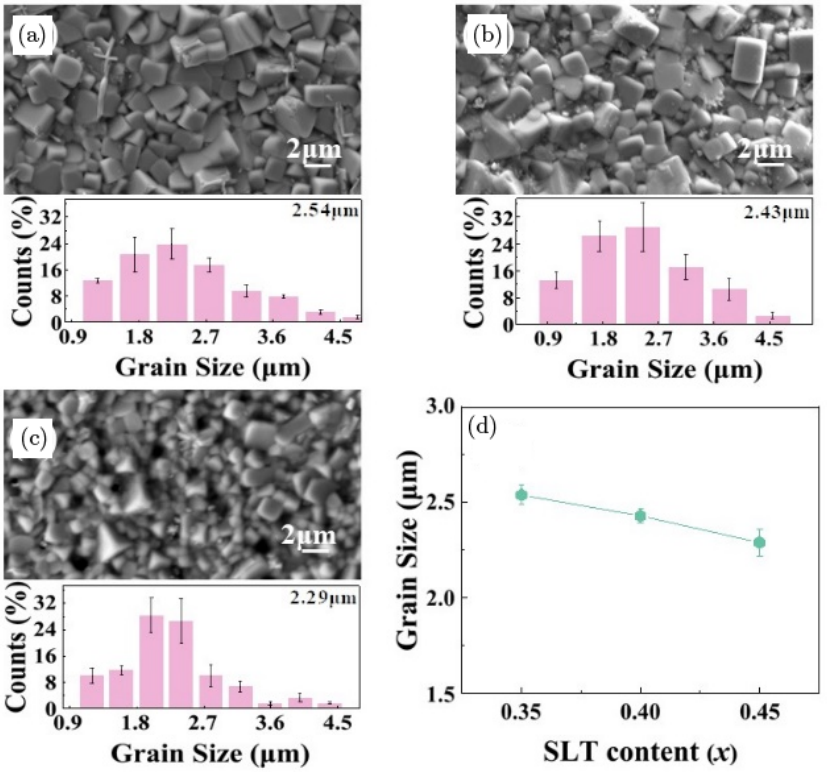

Fig. 2. (a)–(c) SEM images and grain size distribution of $(1-x)$NBT – xSLT ceramics (x = 0.35, 0.4 and 0.45). (d) The average grain size of $(1-x)$NBT – xSLT ceramics.

respectively, as can be seen in the grain size plot at the bottom of Fig. 2. This means that SLT doping can reduce the grain size of the ceramics and the defects, thus increasing the BDS.

As can be seen from Figs. 3(a)–3(c), the ε_r of all ceramics shows a tendency to increase and then decrease with increasing temperature, producing a peak in ε_r. This indicates that at this temperature, the ceramics changed from the ferroelectric phase to the paraelectric phase. As the SLT content increases, the ε_r of the ceramics gradually decreases. A reduced ε_r is beneficial to the increase in energy storage performance, which is due to the decrease in ε_r caused by increased relaxation. As the SLT content increases, local lattice deformation and disruption of ferroelectric long-range ordering produce RFS. RFS leads to a gradual increase in dynamic PNRs and hence enhanced relaxation behavior.[3,32,33] The ε_r and tanδ gradually move toward higher temperatures as the test frequency increases, producing frequency dispersion, which is a manifestation of ceramic relaxation properties.[33,34] Figure 3(d) shows the frequency dependence of the $(1-x)$NBT–xSLT ceramics. As the SLT content increases, ε_r gradually decreases. This is also an indication of progressive strengthening of the relaxation properties of the ceramics due to the increasing SLT content. The overall decrease in ε_r with increasing frequency implies that frequency affects the stability of the ceramics. Of the three components, the 0.45SLT component has the best overall stability.

The Weibull distribution of the ceramic dielectric BDS is shown in Fig. 4(a). The Weibull distribution can be calculated by the equation[35]

$$X_i = \ln\left(E_i\right), \tag{4}$$

where E_i represent the values of specimens of test ceramics. The results for the Weibull distribution of $(1-x)$NBT–xSLT ceramics are shown in Fig. 4(a). The graph shows a good fit of the data points, and all shape parameters (β) are higher than 50 for each composition. Good agreement with the Weibull distribution was found for all test ceramics in the decomposition data. It can be seen that the BDS of the ceramics increases gradually with the increase of SLT content, which is due to the reduction of grain size, which makes the ceramics dense, and these factors make the BDS to have a great improvement.[36] Figure 4(b) shows the P–E loops of the ceramics at the same NBT/SLT ratio. With the increase of SLT, P_{max} decreases, and the ceramics retain the slender shape in general, which is one of the manifestations of the relaxation property. As shown in Fig. 4(c), W_{rec} of $(1-x)$NBT–xSLT ceramics increases significantly from 1.81 J/cm^3 to 2.52 J/cm^3 when the SLT content increases from 0.35 to 0.45. In particular, the 0.55NBT–0.45SLT ceramic has the highest W_{tot} (2.83 J/cm^3) and W_{rec} (2.52 J/cm^3), and maintained a high η (88%). To further elucidate the energy storage performance of the 0.55NBT–0.45SLT ceramic, the P–E loops under the

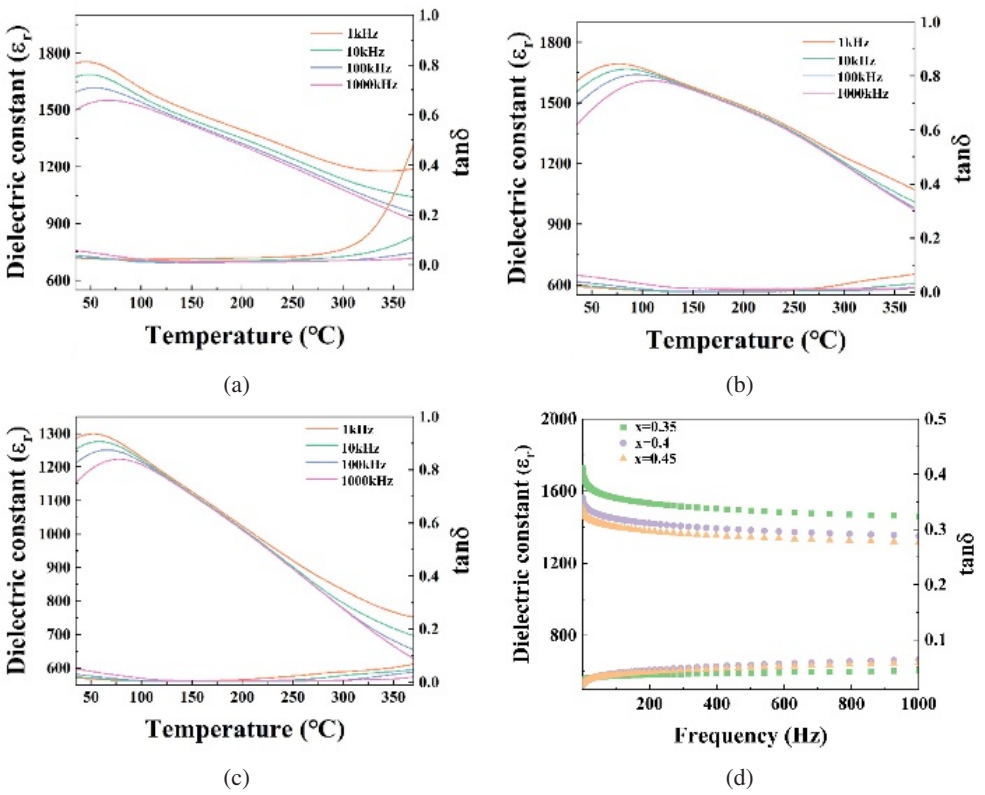

Fig. 3. Dielectric constants and dielectric losses of $(1-x)$NBT – xSLT ceramics (x = 0.35, 0.4 and 0.45): (a)–(c) temperature dependence and (d) frequency dependence.

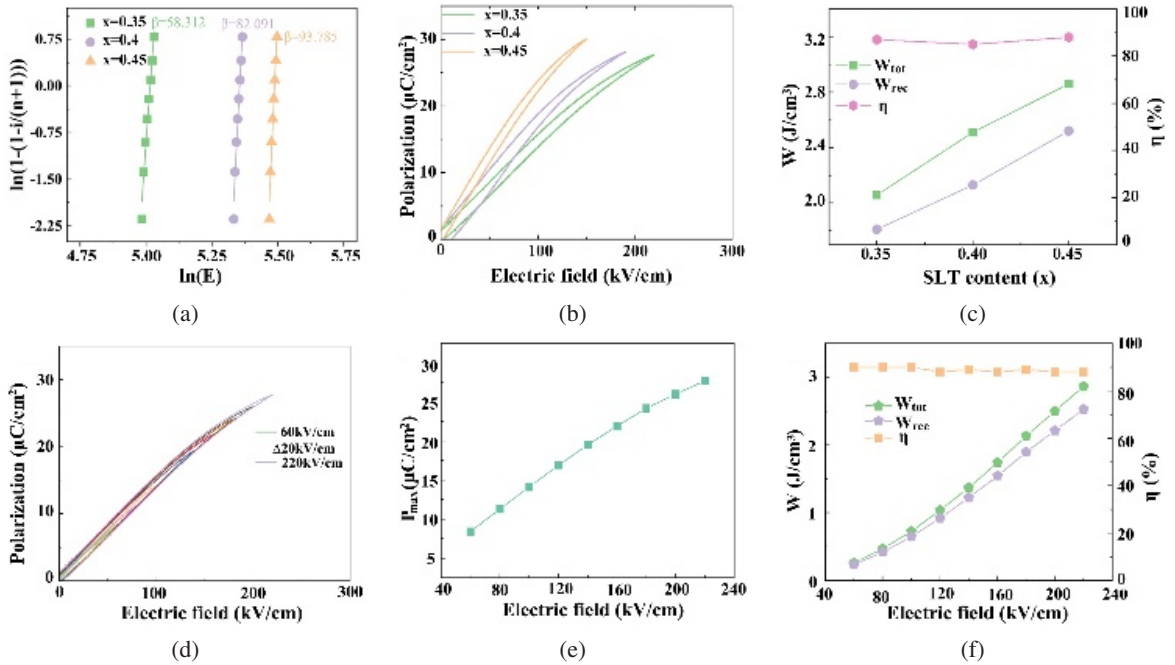

Fig. 4. (a) Weibull distribution function of BDS; (b) P–E loops of $(1-x)$NBT–xSLT ceramics (x=0.35, 0.4 and 0.45); (c) W_{tot}, W_{rec} and η variations with respect to x content; (d) P–E loops of 0.55NBT–0.45SLT ceramic under varying electric field; (e) P_{max} of 0.55NBT–0.45SLT ceramic under different applied electric fields; and (f) W_{tot}, W_{rec} and η as a function of electric field for 0.55NBT–0.45SLT ceramic.

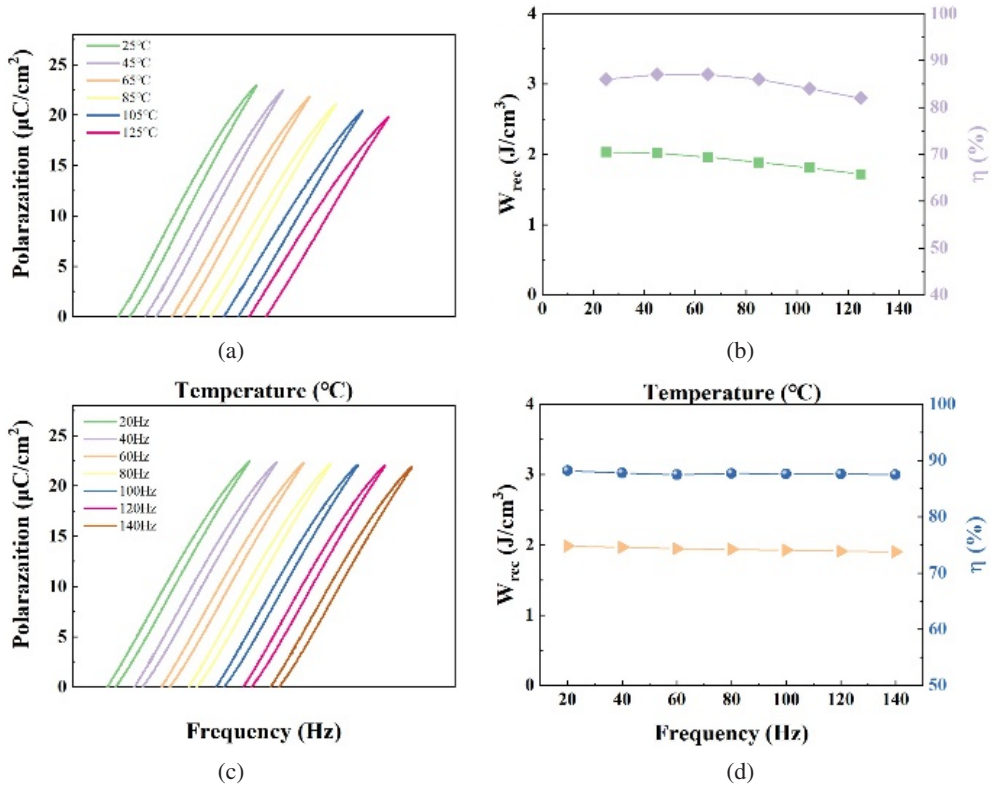

Fig. 5. The 0.55NBT–0.45SLT ceramic results corresponding to the temperature stability and frequency stability under the test conditions.

varying electric field at room temperature (RT) are shown in Figs. 4(d) and 4(e). Both the polarization and energy storage of the ceramics increase gradually with the increase of electric field. The performance of the ceramic is stable under the electric field without polarization or with the sudden change of electric field, which indicates that the ceramic has good stability under low electric field. The rate of increase of P_{max} decreases as the electric field increases from 60 kV/cm to 220 kV/cm. This indicates that as the test electric field increases and gradually approaches the BDS of the ceramic, the polarization of the ceramic also gradually approaches the optimal saturation state. The enhanced P_{max} and BDS are favorable to achieve large W_{rec} in 0.55NBT – 0.45SLT ceramic. The W_{tot}, W_{rec} and η of 0.55NBT – 0.45SLT ceramic under different applied electric fields are shown in Fig. 4(f), respectively. It can be observed that W_{tot} and W_{rec} increase from 0.28 J/cm^3 and 0.25 J/cm^3 to 2.86 J/cm^3 and 2.52 J/cm^3, respectively. η decreases slightly from 90% to 88% with increasing BDS due to enhanced conductivity.

Figure 5 shows the *P–E* curves and energy storage performances of the 0.55NBT–0.45SLT ceramic at different test temperatures and frequencies. The W_{rec} of the ceramic decreases from 2.03 J/cm^3 to 1.72 J/cm^3 in the temperature range of 25–125°C under 200-kV/cm electric field and there is a recoverable energy storage density from 1.98 J/cm^3 to 1.90 J/cm^3 in the frequency range of 20–140 Hz. The slight but insignificant decrease in efficiency in both ranges also shows the high stability of the ceramic.

4. Conclusions

In a nutshell, $(1 - x)$NBT – xSLT lead-free ceramics were prepared by the flow-delay method and the energy storage properties were investigated. A pure perovskite structure and a dense structure were exhibited by the $(1 - x)$NBT – xSLT ceramics. A key role in the reduction of grain size and domain size can be attributed to SLT, which leads to enhanced BDS and relaxation properties. A maximum W_{rec} of 2.86 J/cm^3 and a high η of 88% are obtained for the 0.55NBT – 0.45SLT ceramic. Besides, the 0.55NBT – 0.45SLT ceramic exhibited good temperature and frequency stability. These excellent properties demonstrate the promising potential of the studied dielectric capacitor ceramics for the development of pulsed power systems.

Acknowledgments

The authors acknowledge the support from the Natural Science Foundation of Inner Mongolia (2019ZD12 and 2021JQ06), the Program for "Grassland Talents" Innovation Team of Inner Mongolia (Rare Earth Modified Lead-free Ferroelectric Multilayer Ceramic Capacitors Innovative Talent Team), Scientific and Technological Development

Foundation of the Central Guidance Local (2021ZY0008), Young Talents of Science and Technology in Universities of Inner Mongolia Autonomous Region (NJYT22061), "Light of the West" Talent Training Program of Chinese Academy of Sciences, Key Science and Technology Program of Ordos City (2021EEDSCXQDFZ014), Science and Technology Planning Project of Ordos City (2022YY043) and Science and Technology Planning Project of Inner Mongolia Autonomous Region (2021GG0242).

References

[1]L. Zhao, Q. Liu, J. Gao, S. Zhang and J. F. Li, Lead-free antiferroelectric silver niobate tantalate with high energy storage performance, *Adv. Mater.* **29**, 1701824 (2017).

[2]H. Palneedi, M. Peddigari, G.-T. Hwang, D.-Y. Jeong and J. Ryu, High-performance dielectric ceramic films for energy storage capacitors: Progress and outlook, *Adv. Funct. Mater.* **28**, 1803665 (2018).

[3]Z. Pan, D. Hu, Y. Zhang, J. Liu, B. Shen and J. Zhai, Achieving high discharge energy density and efficiency with NBT-based ceramics for application in capacitors, *J. Mater. Chem. C* **7**, 4072 (2019).

[4]H. Pan, A. Kursumovic, Y. H. Lin, C. W. Nan and J. L. MacManus-Driscoll, Dielectric films for high performance capacitive energy storage: Multiscale engineering, *Nanoscale* **12**, 19582 (2020).

[5]B. Zhang, X. Chen, W. Wu, A. Khesro, P. Liu, M. Mao, K. Song, R. Sun and D. Wang, Outstanding discharge energy density and efficiency of the bilayer nanocomposite films with $BaTiO_3$-dispersed PVDF polymer and polyetherimide layer, *Chem. Eng. J.* **446**, 136926 (2022).

[6]H. Zhang, T. Wei, Q. Zhang, W. Ma, P. Fan, D. Salamon, S.-T. Zhang, B. Nan, H. Tan and Z.-G. Ye, A review on the development of lead-free ferroelectric energy-storage ceramics and multilayer capacitors, *J. Mater. Chem. C* **8**, 16648 (2020).

[7]Z. Fan, L. Li, X. Mei, F. Zhao, H. Li, X. Zhuo, X. Zhang, Y. Lu, L. Zhang and M. Liu, Multilayer ceramic film capacitors for high-performance energy storage: Progress and outlook, *J. Mater. Chem. A* **9**, 9462 (2021).

[8]D. Li, X. Zeng, Z. Li, Z.-Y. Shen, H. Hao, W. Luo, X. Wang, F. Song, Z. Wang and Y. Li, Progress and perspectives in dielectric energy storage ceramics, *J. Adv. Ceram.* **10**, 675 (2021).

[9]P. Zhao, Z. Cai, L. Wu, C. Zhu, L. Li and X. Wang, Perspectives and challenges for lead-free energy-storage multilayer ceramic capacitors, *J. Adv. Ceram.* **10**, 1153 (2021).

[10]D. Wang, Z. Fan, D. Zhou, A. Khesro, S. Murakami, A. Feteira, Q. Zhao, X. Tan and I. M. Reaney, Bismuth ferrite-based lead-free ceramics and multilayers with high recoverable energy density, *J. Mater. Chem. A* **6**, 4133 (2018).

[11]H. Chen, T. N. Cong, W. Yang, C. Tan, Y. Li and Y. Ding, Progress in electrical energy storage system: A critical review, *Prog. Nat. Sci.* **19**, 291 (2009).

[12]H. Qi and R. Zuo, Linear-like lead-free relaxor antiferroelectric $(Bi_{0.5}Na_{0.5})TiO_3$–$NaNbO_3$ with giant energy-storage density/efficiency and super stability against temperature and frequency, *J. Mater. Chem. A* **7**, 3971 (2019).

[13]D. Hu, Z. Pan, X. Zhang, H. Ye, Z. He, M. Wang, S. Xing, J. Zhai, Q. Fu and J. Liu, Greatly enhanced discharge energy density and efficiency of novel relaxation ferroelectric BNT–BKT-based ceramics, *J. Mater. Chem. C* **8**, 591 (2020).

[14]J. Huang, H. Qi, Y. Gao, A. Xie, Y. Zhang, Y. Li, S. Wang and R. Zuo, Expanded linear polarization response and excellent energy-storage properties in $(Bi_{0.5}Na_{0.5})TiO_3$-$KNbO_3$ relaxor antiferroelectrics with medium permittivity, *Chem. Eng. J.* **398**, 125639 (2020).

[15]X. Zhu, Y. Gao, P. Shi, R. Kang, F. Kang, W. Qiao, J. Zhao, Z. Wang, Y. Yuan and X. Lou, Ultrahigh energy storage density in $(Bi_{0.5}Na_{0.5})_{0.65}Sr_{0.35}TiO_3$-based lead-free relaxor ceramics with excellent temperature stability, *Nano Energy* **98**, 107276 (2022).

[16]T. Li, X. Jiang, J. Li, A. Xie, J. Fu and R. Zuo, Ultrahigh energy-storage performances in lead-free $Na_{0.5}Bi_{0.5}TiO_3$-based relaxor antiferroelectric ceramics through a synergistic design strategy, *ACS Appl. Mater. Interfaces* **14**, 22263 (2022).

[17]C. Li, J. Liu, W. Bai, S. Wu, P. Zheng, J. Zhang, Z. Pan and J. Zhai, Superior energy storage performance in $(Bi_{0.5}Na_{0.5})TiO_3$-based lead-free relaxor ferroelectrics for dielectric capacitor application via multiscale optimization design, *J. Mater. Chem. A* **10**, 9535 (2022).

[18]X. Qiao, F. Zhang, D. Wu, B. Chen, X. Zhao, Z. Peng, X. Ren, P. Liang, X. Chao and Z. Yang, Superior comprehensive energy storage properties in $Bi_{0.5}Na_{0.5}TiO_3$-based relaxor ferroelectric ceramics, *Chem. Eng. J.* **388**, 124158 (2020)

[19]J. Shi, X. Chen, X. Li, J. Sun, C. Sun, F. Pang and H. Zhou, Realizing ultrahigh recoverable energy density and superior charge–discharge performance in $NaNbO_3$-based lead-free ceramics via a local random field strategy, *J. Mater. Chem. C* **8**, 3784 (2020).

[20]G. Wang, Z. Lu, J. Li, H. Ji, H. Yang, L. Li, S. Sun, A. Feteira, H. Yang, R. Zuo, D. Wang and I. M. Reaney, Lead-free (Ba,Sr)TiO_3–$BiFeO_3$ based multilayer ceramic capacitors with high energy density, *J. Eur. Ceram. Soc.* **40**, 1779 (2020).

[21]X. Meng, Y. Zhao, Y. Li and X. Hao, Simultaneously achieving ultrahigh energy density and power density in $PbZrO_3$-based antiferroelectric ceramics with field-induced multistage phase transition, *J. Alloys Compd.* **868**, 159149 (2021).

[22]W. Wang, Y. Pu, X. Guo, T. Ouyang, Y. Shi, M. Yang, J. Li, R. Shi and G. Liu, Enhanced energy storage properties of lead-free $(Ca_{0.5}Sr_{0.5})_{1-1.5x}La_xTiO_3$ linear dielectric ceramics within a wide temperature range, *Ceram. Int.* **45**, 14684 (2019).

[23]Y. Lin, D. Li, M. Zhang and H. Yang, $(Na_{0.5}Bi_{0.5})_{0.7}Sr_{0.3}TiO_3$ modified by $Bi(Mg_{2/3}Nb_{1/3})O_3$ ceramics with high energy-storage properties and an ultrafast discharge rate, *J. Mater. Chem. C* **8**, 2258 (2020).

[24]X. Liu, T. Yang and W. Gong, Comprehensively enhanced energy-storage properties in $(Pb_{1-3x/2}La_x)(Zr_{0.995}Ti_{0.005})O_3$ antiferroelectric ceramics via composition optimization, *J.Mater. Chem. C* **9**, 12399 (2021).

[25]J. Li, F. Li, Z. Xu and S. Zhang, Multilayer lead-free ceramic capacitors with ultrahigh energy density and efficiency, *Adv. Mater.* **30**, e1802155 (2018).

[26]P. Chen, W. Cao, T. Li, B. Zhao, J. Zheng and C. Wang, Outstanding energy-storage and charge-discharge performances in $Na_{0.5}Bi_{0.5}TiO_3$ lead-free ceramics via linear additive of $Ca_{0.85}Bi_{0.1}TiO_3$, *Chem. Eng. J.* **435**, 135065 (2022).

[27]X. Qiao, A. Sheng, D. Wu, F. Zhang, B. Chen, P. Liang, J. Wang, X. Chao and Z. Yang, A novel multifunctional ceramic with photoluminescence and outstanding energy storage properties, *Chem. Eng. J.* **408**, 127368 (2021).

[28]Y. Yang, H. Wang, L. Bi, Q. Zheng, G. Fan, W. Jie and D. Lin, High energy storage density and discharging efficiency in La^{3+}/Nb^{5+}-co-substituted $(Bi_{0.5}Na_{0.5})_{0.94}Ba_{0.06}TiO_3$ ceramics, *J. Eur. Ceram. Soc.* **39**, 3051 (2019).

[29]F. Yan, X. Zhou, X. He, H. Bai, S. Wu, B. Shen and J. Zhai, Superior energy storage properties and excellent stability achieved in environment-friendly ferroelectrics via composition design strategy, *Nano Energy* **75**, 105012 (2020).

[30]X. Liu, J. Zhu, Y. Li, T. Yang, X. Hao and W. Gong, High-performance $PbZrO_3$-based antiferroelectric multilayer capacitors based on multiple enhancement strategy, *Chem. Eng. J.* **446**, 136729 (2022).

[31]Z. Ma, Q. Su, J. Zhu, X. Meng, Y. Zhao, G. Xin, Y. Li and X. Hao, Optimization of energy-storage properties for lead-free relaxor-ferroelectric (1-*x*)$Na_{0.5}Bi_{0.5}TiO_3$-*x*$Sr_{0.7}Nd_{0.2}TiO_3$ ceramics, *J. Mater. Sci.* **57**, 217 (2022).

[32]X. Wang, Y. Fan, A. Mostaed, L. Li, A. Feteira, D. Wang, G. Wang and I. M. Reaney, High discharge energy density in novel $K_{1/2}Bi_{1/2}$-TiO_3-$BiFeO_3$ based relaxor ferroelectrics, *J. Eur. Ceram. Soc.* **42**, 7381 (2022).

[33]A. Khesro, F. A. Khan, R. Muhammad, A. Ali, M. Khan and D. Wang, Energy storage performance of Nd^{3+} doped lead-free $BiFeO_3$-$BaTiO_3$-based lead-free ceramics, *Ceram. Int.* **48**, 29938 (2022).

[34]Q. Xu, M. T. Lanagan, X. Huang, J. Xie, L. Zhang, H. Hao and H. Liu, Dielectric behavior and impedance spectroscopy in lead-free BNT–BT–NBN perovskite ceramics for energy storage, *Ceram. Int.* **42**, 9728 (2016).

[35]X. Liu, J. Shi, F. Zhu, H. Du, T. Li, X. Liu and H. Lu, Ultrahigh energy density and improved discharged efficiency in bismuth sodium titanate based relaxor ferroelectrics with A-site vacancy, *J. Materiomics* **4**, 202 (2018).

[36]S. Zhou, Y. Pu, X. Zhao, T. Ouyang, J. Ji, Q. Zhang, S. Sun, R. Sun, J. Li and D. Wang, Excellent dielectric temperature stability and energy storage performance of NBT-based ceramics by introducing high-entropy oxide, *J. Am. Ceram. Soc.* **105**, 4796 (2022).